

BMW/DMZ calculation of the hadronic vacuum polarisation for the muon magnetic moment

**F.M. Stokes,^{a,b,*} M. Davier,^c Z. Fodor,^{d,e,f,b,g,h} F. Frech,^f A.Yu. Kotov,^b
L. Lellouch,ⁱ B. Malaescu,^j S. Mutzel,^{i,k} K.K. Szabo,^{b,f} B.C. Toth,^{b,f} G. Wangⁱ and
Z. Zhang^c for the BMW and DMZ collaborations**

^aSpecial Research Centre for the Subatomic Structure of Matter, Department of Physics,
Adelaide University / Tirkangkaku, Kaurna Country, South Australia 5005, Australia

^bJülich Supercomputing Centre, Forschungszentrum Jülich, D-52428 Jülich, Germany

^cIJCLab, Université Paris-Saclay et CNRS/IN2P3, Orsay, 91405, France

^dPhysics Department, Pennsylvania State University, University Park, PA 16802, USA

^eDepartment of Physics, University of Wuppertal, D-42119 Wuppertal, Germany

^fInstitute for Computational and Data Sciences, Pennsylvania State University,
University Park, PA 16802, USA

^gInstitute for Theoretical Physics, Eötvös University, H-1117 Budapest, Hungary

^hUniversity of California, San Diego, 9500 Gilman Drive, La Jolla, CA 92093, USA

ⁱAix Marseille Univ, Université de Toulon, CNRS, CPT, IPhU, Marseille, France

^jLPNHE, Sorbonne Université, Université Paris Cité, CNRS/IN2P3, Paris, 75252, France

^kLaboratoire de Physique de l'Ecole Normale Supérieure, Mines Paris - PSL,
CNRS, Inria, PSL Research University, Paris, France

E-mail: f.stokes@adelaide.edu.au

For twenty years, a persistent discrepancy between experimental measurements and theoretical calculations of the muon anomalous magnetic moment have provided tantalising hints of new physics. In recent years, improvements to the experimental precision have appeared to make the tension stronger and stronger. However, at the same time, our lattice calculation overturned the theoretical consensus, completely eliminating the tension. I will present the latest results from the Budapest-Marseille-Wuppertal (BMW) and DMZ collaborations, with a determination of the hadronic vacuum polarisation contribution to a precision of 0.45%

The 42nd International Symposium on Lattice Field Theory (LATTICE2025)
2-8 November 2025
Tata Institute of Fundamental Research, Mumbai, India

*Speaker

1. Overview

Almost twenty years ago, physicists at Brookhaven National Laboratory measured the magnetic moment of the muon with a remarkable precision of 0.54 parts per million (ppm) [20]. Since that time, the reference Standard Model prediction for this quantity has exhibited a persistent discrepancy with experiment of more than three sigma [9]. This raises the tantalising possibility of undiscovered forces or elementary particles.

The attention of the world was drawn to this discrepancy when Fermilab presented a brilliant confirmation of Brookhaven’s measurement, which brought the discrepancy to 4.2 sigma [21]. In the meantime a very large-scale lattice QCD calculation of a key theoretical contribution was performed by the Budapest-Marseille-Wuppertal (BMW) collaboration [3], as seen in Fig. 1. This result

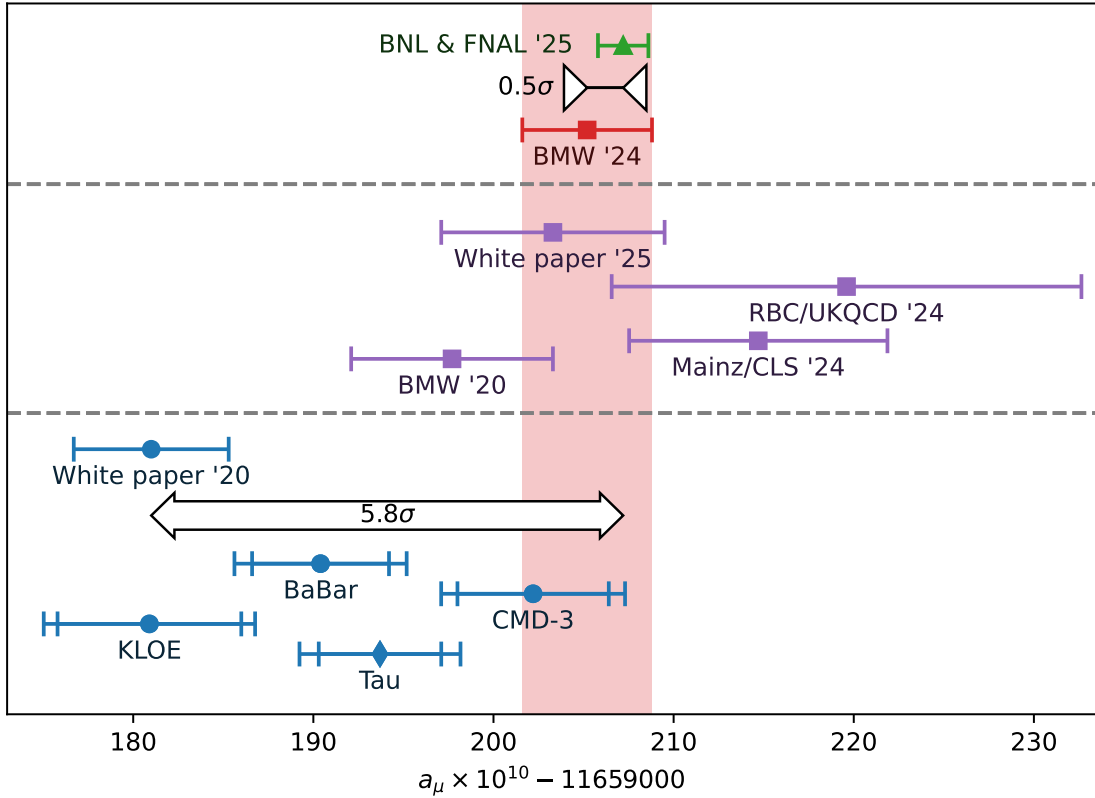


Figure 1: Comparison of Standard Model predictions for the muon anomalous magnetic moment with its measured value, taken from Ref. [1]. The top panel shows a comparison of the world-average experimental measurement of a_μ [2] with the Standard Model prediction obtained by the BMW collaboration [1], denoted by the red band. The middle panel shows a predictions based on the earlier BMW result from Ref. [3] as well as results from two other similar calculations, from RBC/UKQCD [4–6] and Mainz [7], along with the consensus combination of the three from Ref. [8]. The lower panel shows the predictions for $a_\mu^{\text{LO-HVP}}$ obtained in the 2020 approach [9] using specific experimental inputs [10]. These correspond to BaBar [11, 12], KLOE [13–16] and CMD-3 [17], and τ decays [18, 19]. Note, all Standard Model predictions include non-HVP contributions from “White paper ’25”, except for “White paper ’20”.

significantly reduces the difference between theory and experiment, suggesting that new physics may not be needed to explain the experimental results. However, it simultaneously introduces a new discrepancy with the existing data-driven determination of this contribution.

Since then, the experimental [2] results have been updated with significantly improved precision, and the lattice result has been independently confirmed by other lattice collaborations. At the same time, new developments in the data-driven inputs that the lattice calculations replace [17–19] lead to a significant spread in the results depending on what inputs are taken. This has culminated in an updated theory prediction based on the lattice results instead of the data-driven determinations, as seen in Fig. 1.

In these proceedings, I present a new hybrid calculation that combines an update to the most precise lattice results with data-driven inputs in a low-energy region where the observed discrepancies are not present. This new result leads to a prediction that differs from the experimental measurement by only 0.5σ , providing a remarkable validation of the Standard Model to 0.31 ppm.

2. Muon magnetic moment

The quantity under investigation is the so-called anomalous magnetic moment, which is defined in terms of the magnetic moment

$$\vec{\mu}_\mu = g_\mu \left(\frac{q}{2m} \right) \vec{S}.$$

where q is the charge, m is the mass, \vec{S} is the spin, and g is the so-called g factor. The anomalous magnetic moment is the relative deviation of g from its tree-level value of 2.

$$a_\mu = \frac{g_\mu - 2}{2}.$$

This anomalous magnetic moment is measured experimentally by injecting a polarised beam of positively-charged muons into a large magnetic storage ring and observing the decay of the muons into positrons. As the muons cycle around the ring, their magnetic moments precess. The difference between the precession and orbital frequencies is directly related to the anomalous magnetic moment. It can be observed as a variation in the energy distribution of the positrons as the momentum and magnetic moment come in and out of alignment. This is how the experimental result (green triangle) in Fig. 1 was obtained.

The theoretical prediction is dominated by contributions from electromagnetism, which have been computed in perturbation theory up to five loops [22, 23]. The much smaller electroweak contributions have been computed to two loops [24, 25]. These provide extremely precise values for these parts of the total, as can be seen in Table 1.

The remaining contributions come from the strong force, and are: the hadronic vacuum polarisation (HVP), and the hadronic light by light scattering (HLbL). These effects contribute a very small amount to the total value, but they dominate the uncertainty, as seen in Table 1. The work presented in these proceedings computed the HVP, which has the largest contribution to the uncertainty, and is where there have been significant theoretical developments.

Contribution	Value		
$a_\mu^{\text{QED}} \times 10^{10}$	11 658 471.88	\pm	0.02
$a_\mu^{\text{EW}} \times 10^{10}$	15.44	\pm	0.04
$a_\mu^{\text{HVP}} \times 10^{10}$	704.5	\pm	6.1
$a_\mu^{\text{HLbL}} \times 10^{10}$	11.55	\pm	0.99
$a_\mu \times 10^{10}$	11 659 203.3	\pm	6.2

Table 1: Individual contributions to the Standard Model theory consensus from Ref. [8].

3. Hadronic Vacuum Polarisation

Until recently, the accepted approach to obtain the HVP was a data-driven evaluation, based on experimental measurements of hadron production at electron-positron colliders [9, 26–29]. These experimental results were related to the HVP using a dispersive approach.

The HVP can also be calculated in lattice QCD from the vector-vector correlator using the time-momentum representation [30]. It is computed as an integral over Euclidean time,

$$C(t) = \frac{1}{3} \sum_{\mu=1,2,3} \langle J_\mu(t) J_\mu(0) \rangle \quad (1)$$

$$a_\mu^{\text{LO-HVP}} = \alpha^2 \int_0^\infty K(t) C(t) dt \quad (2)$$

where $K(t)$ is a kernel function that encodes the kinematics of the muon.

Historically, lattice QCD results had uncertainties significantly larger than the data-driven results. These uncertainties were large enough that the results were generally consistent with both the data-driven results and the experimental measurement, and hence were unable to weigh in on the discrepancy. This can be seen in Fig. 2.

In 2020, we completed a lattice calculation of the HVP with sub-percent precision [3]. This result was the first lattice calculation with errors comparable to the data-driven evaluations, and was the first that was precise enough to resolve the discrepancy between theory and experiment. To our surprise, this result was significantly larger than the data-driven evaluation, and was close to the experimental measurement.

In 2024, we completed a new calculation [1] that significantly improved upon our 2020 precision, surpassing the data-driven evaluations. Independent calculations from Mainz [7], and RBC/UKQCD [6] confirmed these results, albeit with larger uncertainties.

Our 2020 result was a 3.4 \times increase in precision compared to our previous work [31], and the 2024 update was a further 1.6 \times improvement. Many upgrades were required to reach this level of precision. These improvements were possible by extensive work from many lattice groups around the world in developing and refining the techniques required.

Figure 3 summarises the five main sources of uncertainty in our three calculations, and how they were improved across the three publications to reach the current level of precision. These sources of uncertainty are:

- a the statistical uncertainty;

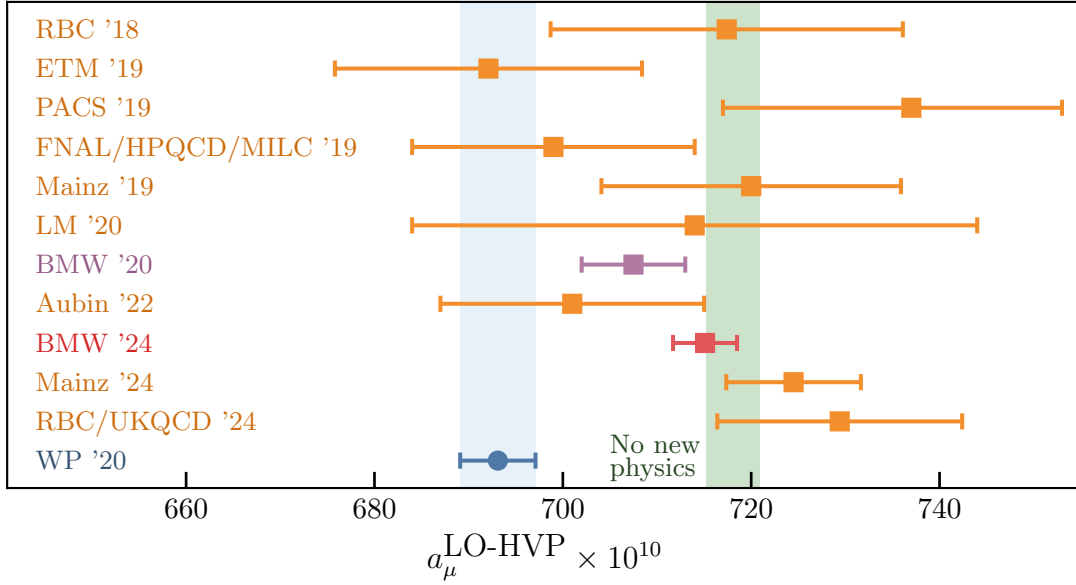


Figure 2: Comparison of lattice values for the leading HVP contribution to the muon magnetic moment. The blue circle is the Standard Model consensus from the 2020 White Paper [9], and the squares are lattice results. The older lattice results [4, 31–37] are consistent with both the Standard Model consensus and the experimental measurement. The four most precise results (from BMW [1, 3], Mainz [7], and RBC/UKQCD [6]) agree with the experimental measurement but not the Standard Model consensus.

- b the effects of the finite volume and temporal extent of the lattice;
- c uncertainties in the continuum extrapolation;
- d uncertainties on the physical values for the inputs used to set the quark masses and scale; and
- e isospin-breaking effects from QED and the up-down quark mass difference.

The dominant uncertainties in the 2017 work came from source (b): uncertainties in removing the effect of the 6 fm box in which we perform our simulations. In 2020, these effects were addressed using dedicated large-volume simulations in an 11 fm box. Our finite-size effects are exponentially suppressed, so these large-volume simulations see dramatically smaller finite-volume effects. The remaining uncertainties due to residual finite volume effects at 11 fm, and to uncertainties in the 11 fm simulation results were small, and mostly affected the large-Euclidean-time tail of the integrand.

Once this uncertainty was reduced, the other sources became significant. In order to bring the final uncertainty down further, we now needed to tackle them. Four further improvements in the 2020 work allowed these reductions:

1. Algorithmic improvements [39, 40] allowed increased statistics, improving the statistical and continuum limit uncertainties.
2. New techniques for the exact treatment of infrared modes [41] improved statistical uncertainty.

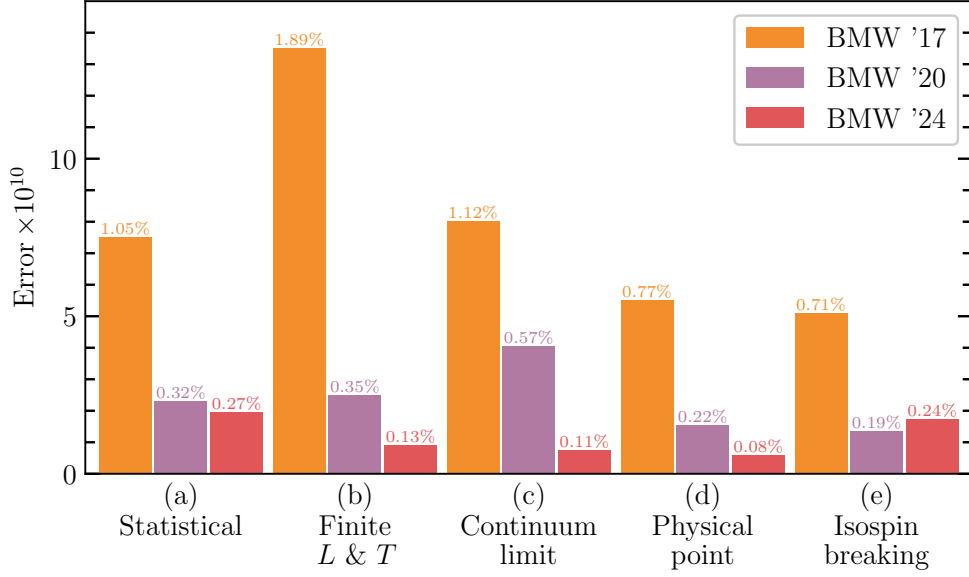


Figure 3: Main uncertainties and their reduction in the BMW collaboration’s successive lattice calculations of $a_\mu^{\text{LO-HVP}}$. Their sources are labelled (a-e) in the text and are given a short descriptive title below the bars in the plot. Their approximate size relative to the total LO-HVP contribution obtained in the present work is also shown. The orange bars on the left of each group correspond to the 2017 BMW result [38], the purple ones in the middle to the 2020 findings [3], and the red ones on the right to the latest BMW preprint [1].

3. A new scale-setting input (the Ω baryon mass) reduced the uncertainty of the physical point.
4. Calculations of all isospin-breaking contributions significantly reduced the associated uncertainty.

In 2024, the analysis was updated with new simulations at a finer lattice spacing, and an overhaul to the analysis procedure. In this work, the Euclidean-time integral was broken up into different windows, and the continuum limit was performed for each window independently. This allowed for a separation of the dominant uncertainties, with different Euclidean times being affected by different sources of uncertainty:

1. The short-distance part has complicated discretisation effects that make the continuum limit challenging, but the statistical errors are small, so it is easy to constrain the form of this extrapolation.
2. The long-distance part has large statistical and finite-size uncertainties.
3. Most of the total value comes from intermediate distances with small statistical errors, and simple well-constrained continuum limits.

Separating out the different distance scales like this not only improved the uncertainties in our lattice calculations, but also allowed us to take a novel “hybrid” approach that brings together the strengths of the lattice and data-driven approach in a complementary way. This approach will be the focus of Section 7 of these proceedings.

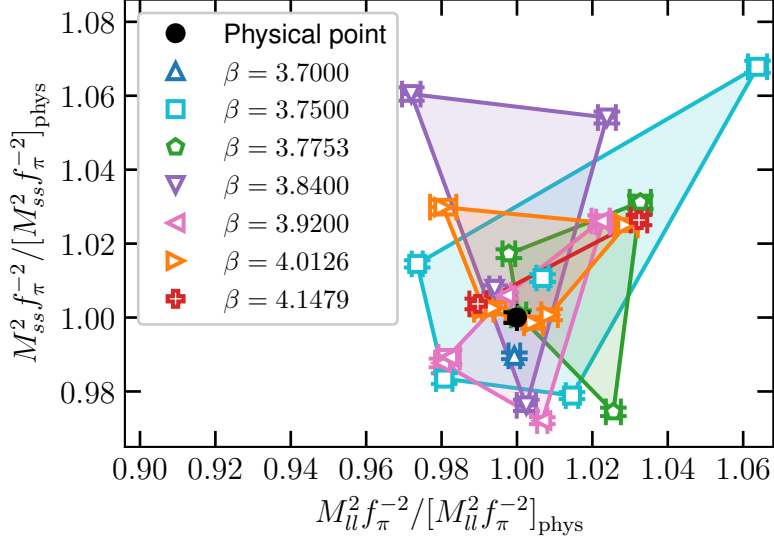


Figure 4: Spread of our ensembles around the physical point, as defined by the masses of the pseudo-scalar mesons M_{ll} and M_{ss} . Different colours denote different lattice spacings. The black point denotes the (isospin-symmetric) physical point, with error bars corresponding to the uncertainties from our determination of M_{ll} and M_{ss} in physical units.

Our 2024 calculation was performed completely blind, with all HVP data multiplied by unknown random numbers before analysis commenced. These blinding factors were only removed once the analysis was finalised and the manuscript was almost complete. This ensured the result was free from any conscious or unconscious biases from any of the researchers. As seen in Fig. 2, this result is in good agreement with the recent lattice results from Mainz [7] and RBC/UKQCD [6], the latest white paper theory consensus [8] and with the experimental measurement [2].

4. Lattice Setup

The simulations for all three works were performed using the tree-level Symanzik gauge action [42] and a one-link staggered fermion action for $2 + 1 + 1$ dynamical quark flavours. Where the gauge link appears in the fermion action, we apply four steps of stout smearing [43] with a smearing parameter of $\rho = 0.125$.

As shown in Fig. 4, the mass of the light ($m_u = m_d = m_l$) and strange (m_s) quarks are chosen to scatter about the physical point. The charm mass parameter is set by the ratio $m_c/m_s = 11.85$, from Ref. [44]. We perform simulations at seven different lattice spacings as listed in Table 2. The finest lattice spacing was added for the 2024 calculation.

Our isospin symmetric simulations all have a spatial extent of approximately 6 fm and a temporal extent of approximately 9 fm. For computing dynamical QED effects, we use a different set of ensembles, some of which have smaller volumes, as listed in Table 3.

To address finite volume effects, we have dedicated large-volume simulations with a spatial extent of approximately 11 fm. These ensembles are computed using the DBW2 gauge action [45]

β	a [fm]	$L/a \times T/a$	am_s	m_s/m_l	#confs
3.7000	0.1315	48×64	0.057291	27.899	904
3.7500	0.1191	56×96	0.049593	28.038	315
			0.049593	26.939	516
			0.051617	29.183	504
			0.051617	28.038	522
			0.055666	28.083	215
3.7753	0.1116	56×84	0.047615	27.843	510
			0.048567	28.400	505
			0.046186	26.469	507
			0.049520	27.852	385
3.8400	0.0952	64×96	0.043194	28.500	510
			0.043194	30.205	436
			0.040750	28.007	1503
			0.039130	26.893	500
3.9200	0.0787	80×128	0.032440	27.679	506
			0.034240	27.502	512
			0.032000	26.512	1001
			0.032440	27.679	327
			0.033286	27.738	1450
			0.034240	27.502	500
4.0126	0.0640	96×144	0.026500	27.634	446
			0.026500	27.124	551
			0.026500	27.634	2248
			0.026500	27.124	1000
			0.027318	27.263	985
			0.027318	28.695	1750
4.1479	0.0483	128×192	0.019370	27.630	2792
			0.019951	27.104	2225

Table 2: List of the ensembles used in our 2024 work, with gauge coupling, lattice spacing, lattice size, strange-quark mass, ratio of strange and light quark masses and number of configurations.

and a one-link staggered fermion action for 2 + 1 dynamical quark flavours, with four steps of HEX smearing [46] applied to the gauge links. This formulation drastically reduces the ultraviolet fluctuations in the gauge configurations, significantly reducing taste-breaking effects in the staggered quarks. These simulations are performed at a single lattice spacing, as listed in Table 4.

5. Analysis Strategy

To obtain the HVP contribution in the continuum physical point, we perform global fits to its lattice spacing and mass dependence. We consider a variety of fit forms and use the variation between the different fit forms as a systematic uncertainty.

β	a [fm]	$L/a \times T/a$	am_s	m_s/m_l	#confs
3.7000	0.1315	24×48	0.057291	27.899	716
		48×64	0.057291	27.899	300
3.7753	0.1116	28×56	0.047615	27.843	887
3.8400	0.0952	32×64	0.043194	28.500	1110
			0.043194	30.205	1072
			0.040750	28.007	1036
			0.039130	26.893	1035

Table 3: List of the ensembles used in our evaluation of dynamical QED effects, with gauge coupling, lattice spacing, lattice size, strange-quark mass, ratio of strange and light quark masses and number of configurations.

β	a [fm]	am_s	m_s/m_l	$L/a \times T/a$	#confs
0.7300	0.112	0.060610	44.971	56×84	7709
				96×96	962
			33.728	56×84	8173
				56×84	813

Table 4: List of ensembles used for our large-volume study in 2020 and 2024, with gauge coupling, lattice spacing, lattice size, strange-quark mass, ratio of strange and light quark masses and number of configurations.

We consider lattice spacing dependence of the form

$$A_0 + A_2 a^2 \alpha_s^\gamma(a) + A_4 a^4 + A_6 a^6 \quad (3)$$

where we get different fit variations by A_6 or A_6 and A_4 to zero, and by choosing different values of γ in the set 0.0, 0.5, 1.0, 1.5, 2.0, 2.5. We consider further variations by excluding some of the coarsest lattice spacings from the fit. When we do this, we always keep at least one more lattice spacing than fit parameters.

We also take into account the quark mass dependence by considering terms linear in the variables

$$X_l = M_{ll}^2 w_0^2 - [M_{ll}^2 w_0^2]_{\text{phys}} \quad \text{and} \quad X_s = M_{ss}^2 w_0^2 - [M_{ss}^2 w_0^2]_{\text{phys}} \quad (4)$$

which describe the deviation from the physical light and strange quark mass respectively. Finally, we make a number of variations to the input into the fits, for example varying the physical inputs within their uncertainties.

Once we have all of these fits, how do we combine them to get a value and uncertainty? We need to take into account the quality of the fits as well as the number of parameters in order to avoid over- or under-fitting. To do this, we use a weight based on a version of the Akaike information criterion (AIC) [47–49] with modifications derived in Ref. [3] to account for differing numbers of data points in different fits:

$$w = \exp \left[-\frac{1}{2} \left(\chi^2 + 2n_{\text{par}} - n_{\text{data}} \right) \right]. \quad (5)$$

This weight is computed from the χ^2 of the fit, the number of parameters n_{par} , and the number of data points included in the fit n_{data} .

Using jackknife resampling, we obtain the statistical uncertainties on each fit and combine the corresponding statistical distributions with their AIC weights to form a total CDF. Then we obtain a central value from the median of this CDF and a total uncertainty (combined statistical and systematic) from the width of this distribution. Specifically, we look at the one (and two) sigma confidence band, and take half (a quarter) of its width as the uncertainty. To avoid any non-gaussianity of this distribution leading to underestimated uncertainties, we take the larger of these two uncertainty estimates.

6. Euclidean-Time Windows

As discussed in Section 3, the various challenges facing this calculation affect different Euclidean time ranges differently. We can take advantage of this by breaking the integral up into different Euclidean time windows [4]. We do this by modifying the kernel function $K(t)$ to focus

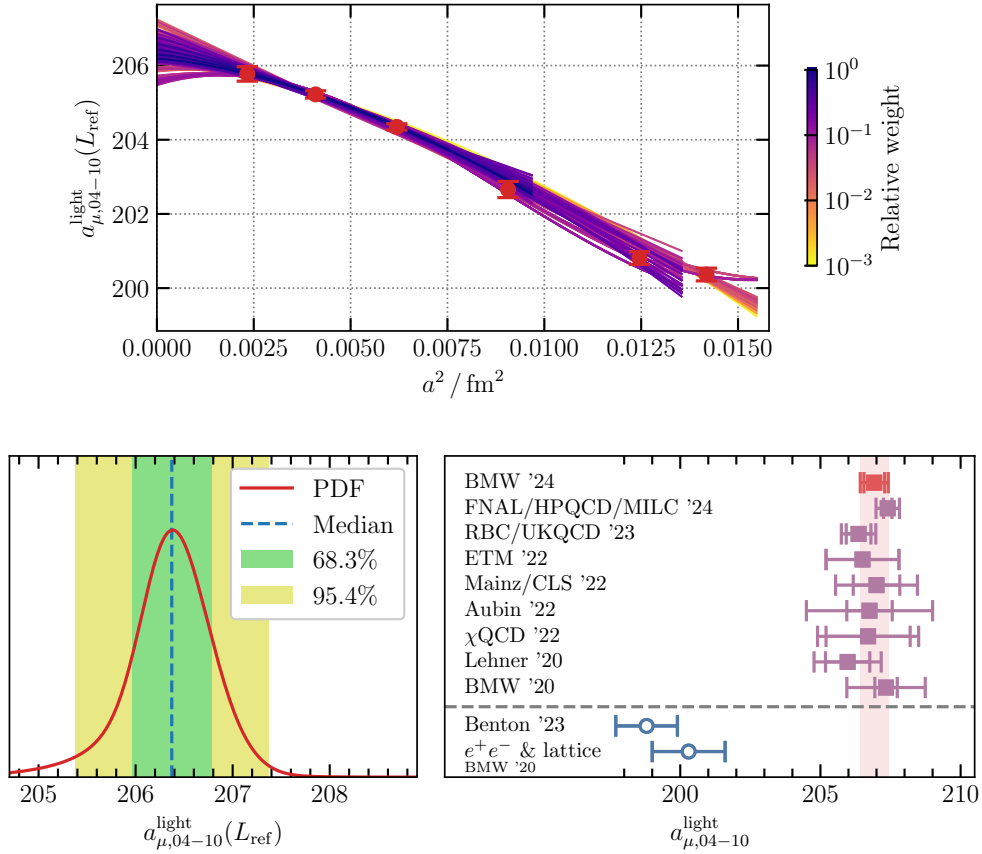


Figure 5: Light-connected window observable $a_{\mu,04-10}^{\text{light}}$. Top: continuum extrapolations, coloured according to the weight of the fit in our analysis. Lower left: the probability distribution function, which shows a single well-defined peak. The shaded bands correspond to the one- and two-sigma confidence bands. Lower right: we compare our result with others from the literature, both lattice [3, 5, 36, 37, 50–53] and data-driven [3, 54].

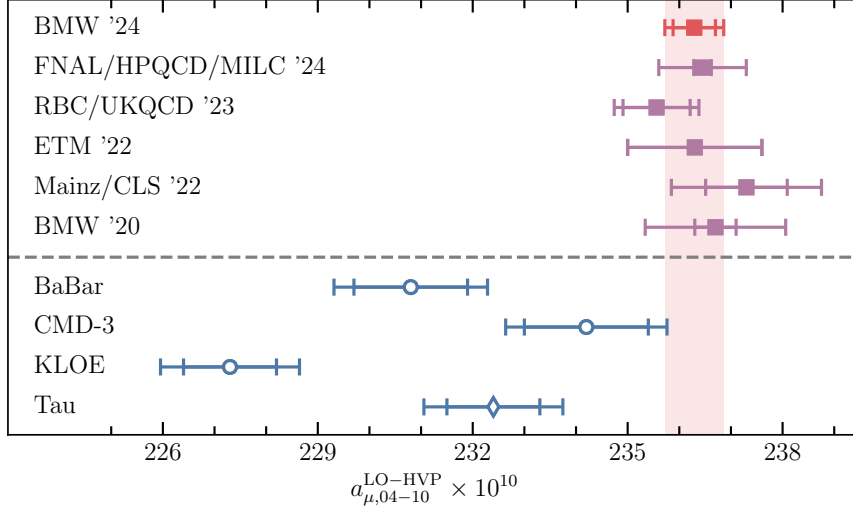


Figure 6: Comparison of our full intermediate-window results, $a_{\mu,04-10}^{LO-HVP}$, with others in the literature. In the top panel, we show lattice results [1, 3, 5, 51–53]. In the lower panel, we show data-driven results [10] that use the measurements of the two-pion spectrum obtained in individual electron-positron annihilation experiments and in τ -decays, as explained in Ref. [10].

on specific regions in t . It is straightforward to compute the effect of such a modification upon the data-driven calculation, so calculations of particular windows can be compared to equivalent data-driven results.

One window of particular interest focuses on an intermediate region of Euclidean time between 0.4 fm and 1.0 fm. This specific window is particularly accessible to lattice QCD calculations, and has been computed by many collaborations, with excellent agreement as shown in Fig. 5. This window emphasises energies near the rho resonance, which is the region in which tension between data-driven inputs is greatest. This can be seen from the spread between data-driven determinations based on different experiments seen in Fig. 6.

The short distance part below 0.4 fm exhibits important logarithmic discretisation effects. Perturbation theory agrees well with the lattice results below 0.3 fm, as seen in Fig. 7. It successfully quantifies these logarithmic effects, so we use a perturbation theory motivated fit form to account for them. The results for this window are shown in Fig. 8, including a comparison to other lattice groups' calculations that shows good agreement.

7. Hybrid Approach

The long-distance region is very sensitive to finite-size effects, and to statistical uncertainties, particularly in the region beyond 2.8 fm. This makes it the most challenging part of the integral to compute in lattice QCD. It only contributes about 5% of the final value, but it contributes significantly to the final uncertainty.

However, it turns out that this very-long-distance tail is dominated by low energy states, well below the rho resonance. In particular, the experimental tensions that plague the data-driven

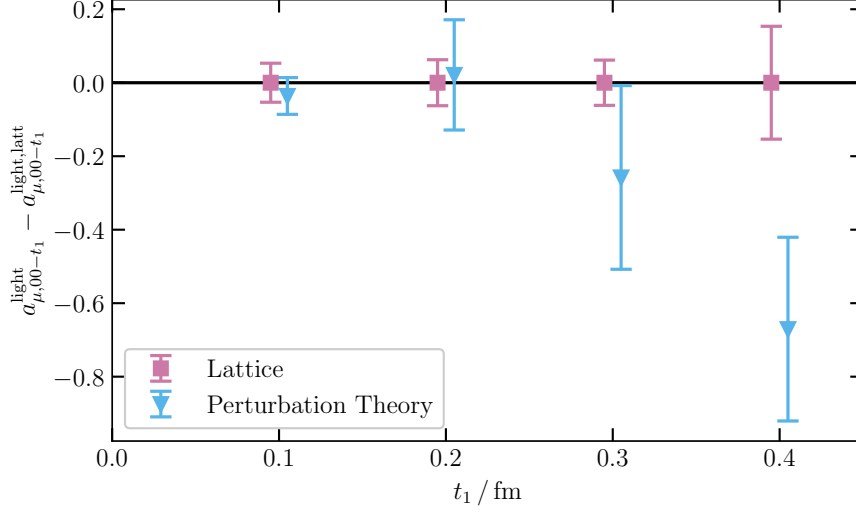


Figure 7: Comparison of the short-distance window observables $a_{\mu,00-t_1}^{\text{light}}$ between the lattice results and those obtained from perturbation theory. For ease of comparison, the central value of the lattice results has been subtracted off, and a slight horizontal offset has been applied.

approach in the region of the rho peak are significantly suppressed by this kernel. This makes this window one of the most reliable to compute in the data-driven approach. As shown in Fig. 9, the data-driven results based on different experiments are in good agreement with one another and also with the lattice result.

This means we can take advantage of the complementary strengths of the lattice calculation and data-driven determination by adopting a hybrid approach. By replacing this small part of the integral with a data-driven result, the finite-size uncertainty is significantly reduced, and the statistical and physical point uncertainties are also improved. At the same time, we avoid sensitivity to the data-driven discrepancies and restrict the data-driven contribution to less than 5% of the total.

To account for possible sensitivities to how the data-driven part of the hybrid calculation is performed, we include additional uncertainties associated with variations in the data-driven procedure, specifically:

- whether the different experiments are averaged before or after integrating over the energy spectrum,
- whether additional experiments that only cover part of the energy range are included or not,
- the effect of including or excluding the CMD3 experiment, and
- the difference between the BaBar and KLOE experiments on the rho peak.

Including these additional systematics gives an overestimate of the final uncertainties, as it will multiply count several sources of uncertainties. It ends up increasing the uncertainty on the tail contribution by a factor of two but has a negligible effect on the uncertainty of the final result for a_μ .

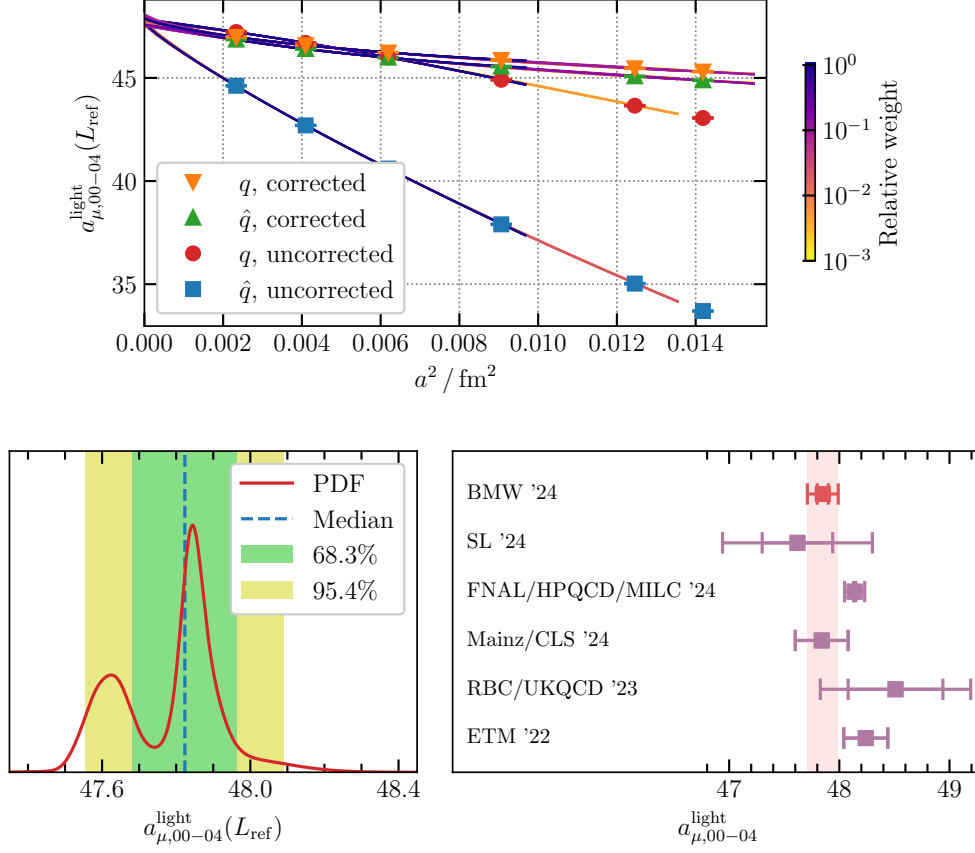


Figure 8: Light-connected window observable $a_{\mu,00-04}^{\text{light}}$. Top: continuum extrapolations, coloured according to the weight of the fit in our analysis. We plot fits with two different kernel functions, denoted by q and \hat{q} , which correspond to two different discretisations for the momentum, and also show fits to data either corrected or not corrected by tree-level perturbation theory. Lower left: the probability distribution function, which displays two dominant peaks, corresponding to the variation between q and \hat{q} in the uncorrected case. Lower right: we compare our result with others from the literature [5, 52, 53, 55, 56].

The final Euclidean time region from 1.0 fm to 2.8 fm is then computed in lattice QCD. The results are shown in Fig. 10.

8. Scale Setting

The 2020 result used the mass of the Omega baryon to set the physical scale. Our most precise result for the Omega mass uses a generalised eigenvalue problem (GEVP) to isolate the ground state. We use a combination of spatial Wuppertal smearing [58] and the Generalised-Pencil-of-Function approach [59] to construct a 6×6 correlation matrix. The GEVP successfully extracts four states: the ground state Omega, and three excited states that have energies consistent with the expected resonances, based on experimental results [57] and quark model predictions [60]. This allows for a clean and clear ground state plateau as shown in Fig. 11. However, this GEVP does not isolate

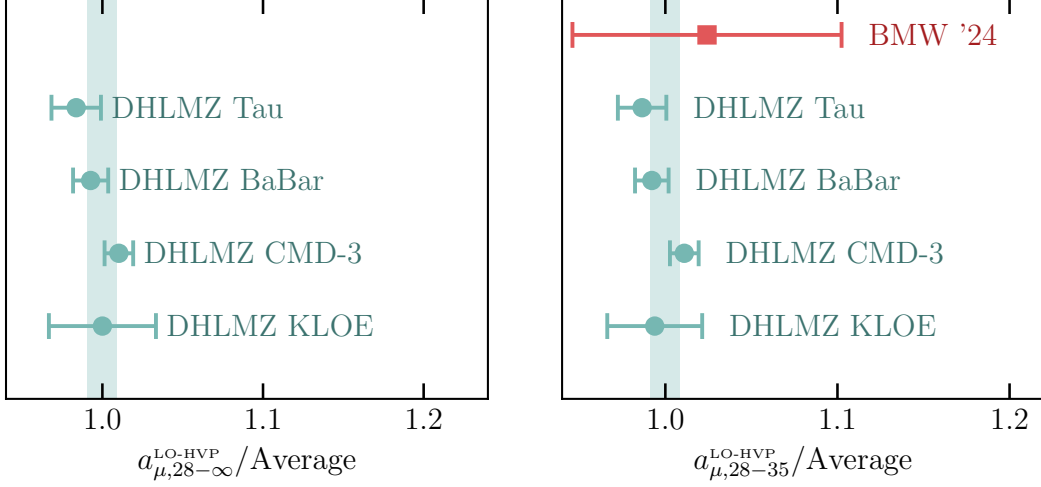


Figure 9: A comparison of data-driven results for the long-distance tail of the HVP with two-pion production data restricted to specific experimental data sets, including results from tau decays [1]. The shaded bands represent an average of the data-driven points, and all points are relative to the central value of that average. Left: the entire tail from 2.8 fm to infinity. Right: a comparison with lattice for the part of the tail from 2.8 fm to 3.5 fm. The scatter of the individual results is consistent with their uncertainties, and the lattice result agrees well, although its errors are larger. The shaded band is a combination of the data-driven points.

the nearby $K\Xi$ scattering states, and hence there are potential contaminations from these states that may not be controlled.

To avoid this potential unquantified systematic, we have since moved to a scale setting based on the pion decay constant f_π . This required a determination of the radiative corrections to leptonic decays, which were partly taken from the electro-quenched calculation of Ref. [67], and partly computed in our 2024 work. This analysis was done completely blinded, and gave a result that was completely consistent with our M_Ω scale, as seen in Fig. 12.

9. Change From 2020

It is useful to quantify the agreement or disagreement between our 2020 and 2024 results. The major changes that have occurred between the two are:

- the addition of a new, finer lattice spacing,
- subdivision of the integral into individual windows,
- the inclusion of fits that are cubic in a^2 (in 2020, there were only linear and quadratic),
- changing the quantity used for scale setting (M_Ω to f_π), and
- the replacement of the tail with a data-driven result (significantly reducing finite-size effect).

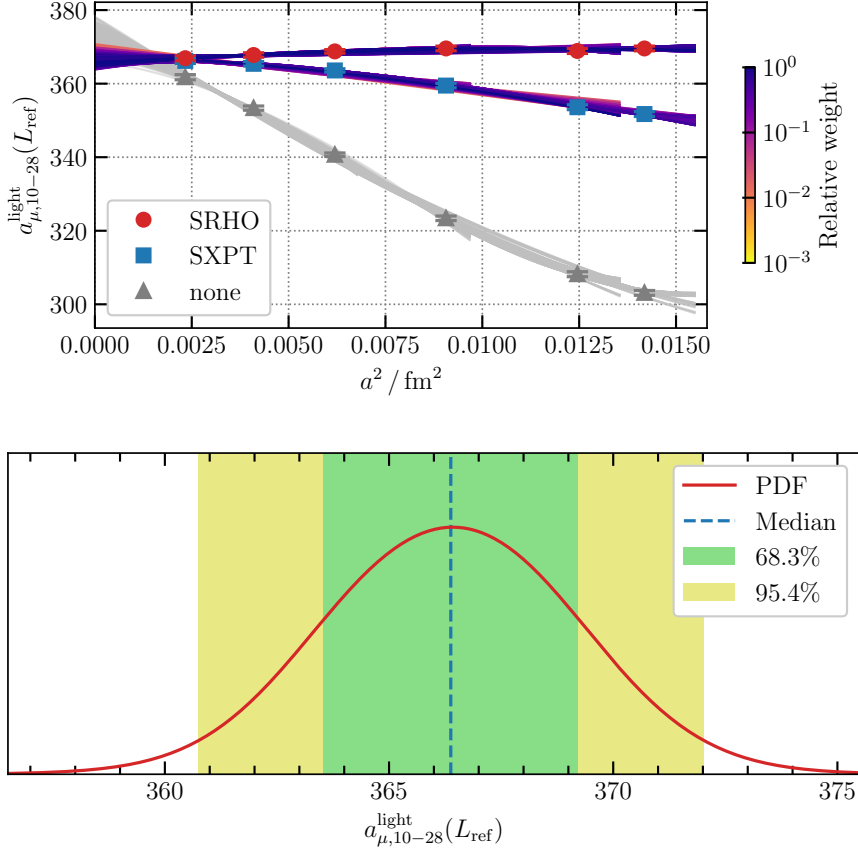


Figure 10: Light-connected window observable $a_{\mu,10-28}^{\text{light}}$. Top: continuum extrapolations, coloured according to the weight of the fit in our analysis, with no, NNLO XPT and SRHO taste improvements. Bottom: the probability distribution function.

With all of these factors taken together, we estimate the correlated difference between the old and new results to be $7.6(5.2) \times 10^{-10}$. This means the new result is 1.5σ higher. This is entirely consistent with expected statistical fluctuations.

10. Conclusion

Recent lattice QCD results have surpassed the precision of all other theoretical predictions of the hadronic vacuum polarisation contribution to the muon magnetic moment. When taken together with the latest theory consensus for the other contributions [8], these results show excellent agreement with the latest experimental measurements [2]. This a remarkable success for quantum field theory, bringing together diverse computational tools to include all aspects of the Standard Model in a single calculation that validates the Standard Model to 0.31 ppm.

11. Acknowledgements

Figures in this work were produced with the aid of Matplotlib [68].

We gratefully acknowledge GCS e.V., GENCI (grant 502275), EuroHPC Joint Undertaking (grants EXT-2023E02-063, EXT-2024E02-109) and NCMAS for providing computer time on SuperMUC-NG at LRZ; HAWK and HUNTER at HLRS; JUWELS, JURECA and JUPITER at FZJ; Joliot-Curie/Irène Rome at TGCC; Jean-Zay V100 at IDRIS; Adastra at CINES; Leonardo at CINECA; LUMI at CSC; Gadi at NCI; and Setonix at PSC. We also gratefully acknowledge grants AMX-18-ACE-005, AMX-22-RE-AB-052, NW21-024-A, BMBF-05P21PXFCA, ERC-MUON-101054515, NW21-024-B, DOE-0000278885 and DE-SC0025025; and the Ramsay Fellowship.

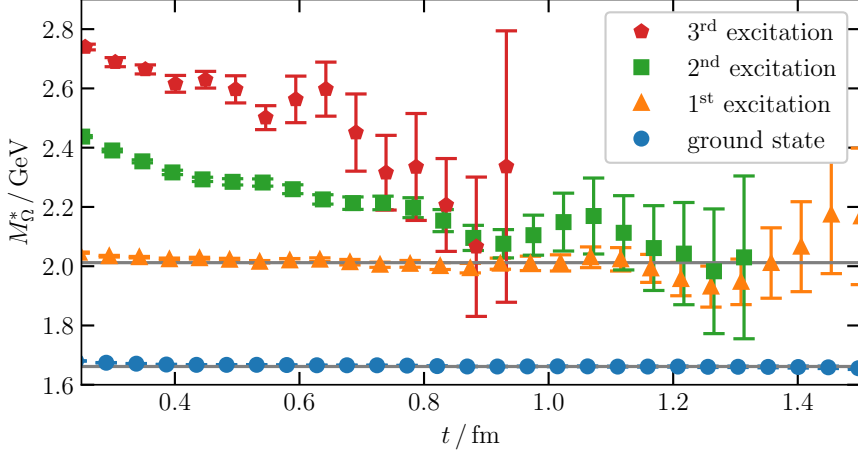


Figure 11: Ground state Ω baryon effective mass obtained through a GEVP, along with three excited states, at $\beta = 4.1479$. The band through the ground state is from a single-exponential fit to the projected ground state propagator. The line through the first excitation shows the mass of the Ω excitation observed at Belle [57].

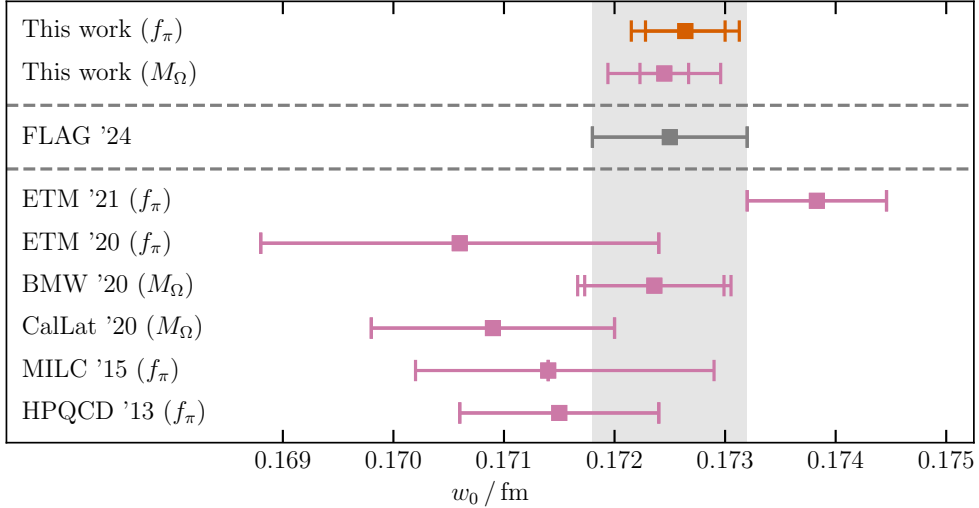


Figure 12: Comparison of the gradient-flow scale w_0 using either M_Ω or f_π for scale setting. The lower panel shows earlier determinations [3, 61–65] and the grey band shows the latest FLAG average [66].

References

- [1] A. Boccaletti et al., *High precision calculation of the hadronic vacuum polarisation contribution to the muon anomaly*, [arXiv:2407.10913](#).
- [2] MUON G-2 collaboration, *Measurement of the Positive Muon Anomalous Magnetic Moment to 127 ppb*, *Phys. Rev. Lett.* **135** (2025) 101802 [[arXiv:2506.03069](#)].
- [3] S. Borsanyi et al., *Leading hadronic contribution to the muon magnetic moment from lattice QCD*, *Nature* **593** (2021) 51 [[arXiv:2002.12347](#)].
- [4] RBC, UKQCD collaboration, *Calculation of the hadronic vacuum polarization contribution to the muon anomalous magnetic moment*, *Phys. Rev. Lett.* **121** (2018) 022003 [[arXiv:1801.07224](#)].
- [5] RBC, UKQCD collaboration, *Update of Euclidean windows of the hadronic vacuum polarization*, *Phys. Rev. D* **108** (2023) 054507 [[arXiv:2301.08696](#)].
- [6] RBC, UKQCD collaboration, *Long-Distance Window of the Hadronic Vacuum Polarization for the Muon $g - 2$* , *Phys. Rev. Lett.* **134** (2025) 201901 [[arXiv:2410.20590](#)].
- [7] D. Djukanovic, G. von Hippel, S. Kuberski, H.B. Meyer, N. Miller, K. Ottnad et al., *The hadronic vacuum polarization contribution to the muon $g - 2$ at long distances*, [arXiv:2411.07969](#).
- [8] R. Aliberti et al., *The anomalous magnetic moment of the muon in the Standard Model: an update*, *Phys. Rept.* **1143** (2025) 1 [[arXiv:2505.21476](#)].
- [9] T. Aoyama et al., *The anomalous magnetic moment of the muon in the Standard Model*, *Phys. Rept.* **887** (2020) 1 [[arXiv:2006.04822](#)].
- [10] M. Davier, A. Hoecker, A.-M. Lutz, B. Malaescu and Z. Zhang, *Tensions in $e^+e^- \rightarrow \pi^+\pi^-(\gamma)$ measurements: the new landscape of data-driven hadronic vacuum polarization predictions for the muon $g - 2$* , *Eur. Phys. J. C* **84** (2024) 721 [[arXiv:2312.02053](#)].
- [11] BABAR collaboration, *Precise measurement of the $e^+e^- \rightarrow \pi^+\pi^-(\gamma)$ cross section with the Initial State Radiation method at BABAR*, *Phys. Rev. Lett.* **103** (2009) 231801 [[arXiv:0908.3589](#)].
- [12] BABAR collaboration, *Precise Measurement of the $e^+e^- \rightarrow \pi^+\pi^-(\gamma)$ Cross Section with the Initial-State Radiation Method at BABAR*, *Phys. Rev. D* **86** (2012) 032013 [[arXiv:1205.2228](#)].
- [13] KLOE collaboration, *Measurement of $\sigma(e^+e^- \rightarrow \pi^+\pi^-\gamma(\gamma))$ and the dipion contribution to the muon anomaly with the KLOE detector*, *Phys. Lett. B* **670** (2009) 285 [[arXiv:0809.3950](#)].

- [14] KLOE collaboration, *Measurement of $\sigma(e^+e^- \rightarrow \pi^+\pi^-)$ from threshold to 0.85 GeV^2 using Initial State Radiation with the KLOE detector*, *Phys. Lett. B* **700** (2011) 102 [arXiv:1006.5313].
- [15] KLOE collaboration, *Precision measurement of $\sigma(e^+e^- \rightarrow \pi^+\pi^-\gamma)/\sigma(e^+e^- \rightarrow \mu^+\mu^-\gamma)$ and determination of the $\pi^+\pi^-$ contribution to the muon anomaly with the KLOE detector*, *Phys. Lett. B* **720** (2013) 336 [arXiv:1212.4524].
- [16] KLOE-2 collaboration, *Combination of KLOE $\sigma(e^+e^- \rightarrow \pi^+\pi^-\gamma(\gamma))$ measurements and determination of $a_\mu^{\pi^+\pi^-}$ in the energy range $0.10 < s < 0.95 \text{ GeV}^2$* , *JHEP* **03** (2018) 173 [arXiv:1711.03085].
- [17] CMD-3 collaboration, *Measurement of the $e+e^- \rightarrow \pi+\pi^-$ cross section from threshold to 1.2 GeV with the CMD-3 detector*, *Phys. Rev. D* **109** (2024) 112002 [arXiv:2302.08834].
- [18] M. Davier, A. Hoecker, G. Lopez Castro, B. Malaescu, X. Mo, G. Toledo Sanchez et al., *The Discrepancy Between tau and $e+e^-$ Spectral Functions Revisited and the Consequences for the Muon Magnetic Anomaly*, *Eur. Phys. J. C* **66** (2010) 127 [arXiv:0906.5443].
- [19] M. Davier, A. Höcker, B. Malaescu, C.-Z. Yuan and Z. Zhang, *Update of the ALEPH non-strange spectral functions from hadronic τ decays*, *Eur. Phys. J. C* **74** (2014) 2803 [arXiv:1312.1501].
- [20] MUON G-2 collaboration, *Final Report of the Muon E821 Anomalous Magnetic Moment Measurement at BNL*, *Phys. Rev. D* **73** (2006) 072003 [hep-ex/0602035].
- [21] MUON G-2 collaboration, *Measurement of the Positive Muon Anomalous Magnetic Moment to 0.46 ppm* , *Phys. Rev. Lett.* **126** (2021) 141801 [arXiv:2104.03281].
- [22] T. Aoyama, T. Kinoshita and M. Nio, *Theory of the Anomalous Magnetic Moment of the Electron*, *Atoms* **7** (2019) 28.
- [23] T. Aoyama, M. Hayakawa, T. Kinoshita and M. Nio, *Complete Tenth-Order QED Contribution to the Muon $g-2$* , *Phys. Rev. Lett.* **109** (2012) 111808 [arXiv:1205.5370].
- [24] A. Czarnecki, W.J. Marciano and A. Vainshtein, *Refinements in electroweak contributions to the muon anomalous magnetic moment*, *Phys. Rev. D* **67** (2003) 073006 [hep-ph/0212229].
- [25] C. Gnendiger, D. Stöckinger and H. Stöckinger-Kim, *The electroweak contributions to $(g-2)_\mu$ after the Higgs boson mass measurement*, *Phys. Rev. D* **88** (2013) 053005 [arXiv:1306.5546].
- [26] M. Davier, A. Hoecker, B. Malaescu and Z. Zhang, *Reevaluation of the hadronic vacuum polarisation contributions to the Standard Model predictions of the muon $g-2$ and $\alpha(M_Z^2)$ using newest hadronic cross-section data*, *Eur. Phys. J. C* **77** (2017) 827 [arXiv:1706.09436].
- [27] A. Keshavarzi, D. Nomura and T. Teubner, *Muon $g-2$ and $\alpha(M_Z^2)$: a new data-based analysis*, *Phys. Rev. D* **97** (2018) 114025 [arXiv:1802.02995].

- [28] G. Colangelo, M. Hoferichter and P. Stoffer, *Two-pion contribution to hadronic vacuum polarization*, *JHEP* **02** (2019) 006 [[arXiv:1810.00007](#)].
- [29] M. Hoferichter, B.-L. Hoid and B. Kubis, *Three-pion contribution to hadronic vacuum polarization*, *JHEP* **08** (2019) 137 [[arXiv:1907.01556](#)].
- [30] D. Bernecker and H.B. Meyer, *Vector Correlators in Lattice QCD: Methods and applications*, *Eur. Phys. J.* **A47** (2011) 148 [[arXiv:1107.4388](#)].
- [31] BUDAPEST-MARSEILLE-WUPPERTAL collaboration, *Hadronic vacuum polarization contribution to the anomalous magnetic moments of leptons from first principles*, *Phys. Rev. Lett.* **121** (2018) 022002 [[arXiv:1711.04980](#)].
- [32] D. Giusti and S. Simula, *Lepton anomalous magnetic moments in Lattice QCD+QED*, *PoS LATTICE2019* (2019) 104 [[arXiv:1910.03874](#)].
- [33] PACS collaboration, *Hadronic vacuum polarization contribution to the muon $g - 2$ with $2+1$ flavor lattice QCD on a larger than $(10\text{ fm})^4$ lattice at the physical point*, *Phys. Rev. D* **100** (2019) 034517 [[arXiv:1902.00885](#)].
- [34] FERMILAB LATTICE, LATTICE-HPQCD, MILC collaboration, *Hadronic-vacuum-polarization contribution to the muon's anomalous magnetic moment from four-flavor lattice QCD*, *Phys. Rev. D* **101** (2020) 034512 [[arXiv:1902.04223](#)].
- [35] A. Gerardin, M. Ce, G. von Hippel, B. Horz, H.B. Meyer, D. Mohler et al., *The leading hadronic contribution to $(g - 2)_\mu$ from lattice QCD with $N_f = 2 + 1$ flavours of $O(a)$ improved Wilson quarks*, *Phys. Rev. D* **100** (2019) 014510 [[arXiv:1904.03120](#)].
- [36] C. Lehner and A.S. Meyer, *Consistency of hadronic vacuum polarization between lattice QCD and the R-ratio*, *Phys. Rev. D* **101** (2020) 074515 [[arXiv:2003.04177](#)].
- [37] C. Aubin, T. Blum, M. Golterman and S. Peris, *Muon anomalous magnetic moment with staggered fermions: Is the lattice spacing small enough?*, *Phys. Rev. D* **106** (2022) 054503 [[arXiv:2204.12256](#)].
- [38] BUDAPEST-MARSEILLE-WUPPERTAL collaboration, *Hadronic vacuum polarization contribution to the anomalous magnetic moments of leptons from first principles*, *Phys. Rev. Lett.* **121** (2018) 022002 [[arXiv:1711.04980](#)].
- [39] G.S. Bali, S. Collins and A. Schafer, *Effective noise reduction techniques for disconnected loops in Lattice QCD*, *Comput. Phys. Commun.* **181** (2010) 1570 [[arXiv:0910.3970](#)].
- [40] T. Blum, T. Izubuchi and E. Shintani, *New class of variance-reduction techniques using lattice symmetries*, *Phys. Rev. D* **88** (2013) 094503 [[arXiv:1208.4349](#)].
- [41] H. Neff, N. Eicker, T. Lippert, J.W. Negele and K. Schilling, *On the low fermionic eigenmode dominance in QCD on the lattice*, *Phys. Rev. D* **64** (2001) 114509 [[hep-lat/0106016](#)].

- [42] M. Luscher and P. Weisz, *On-Shell Improved Lattice Gauge Theories*, *Commun. Math. Phys.* **97** (1985) 59.
- [43] C. Morningstar and M.J. Peardon, *Analytic smearing of SU(3) link variables in lattice QCD*, *Phys. Rev.* **D69** (2004) 054501 [[hep-lat/0311018](#)].
- [44] C. McNeile, C.T.H. Davies, E. Follana, K. Hornbostel and G.P. Lepage, *High-Precision c and b Masses, and QCD Coupling from Current-Current Correlators in Lattice and Continuum QCD*, *Phys. Rev. D* **82** (2010) 034512 [[arXiv:1004.4285](#)].
- [45] T. Takaishi, *Heavy quark potential and effective actions on blocked configurations*, *Phys. Rev.* **D54** (1996) 1050.
- [46] T.A. DeGrand, A. Hasenfratz and T.G. Kovacs, *Improving the chiral properties of lattice fermions*, *Phys. Rev.* **D67** (2003) 054501 [[hep-lat/0211006](#)].
- [47] H. Akaike, *Information theory and an extension of the maximum likelihood principle*, in *2nd International Symposium on Information Theory*, B. Petrov and F. Csaki, eds., pp. 267–281, Akademiai Kiado, Budapest, 1973.
- [48] H. Akaike, *A new look at the statistical model identification*, *IEEE Trans. Automatic Control* **19** (1974) 716.
- [49] H. Akaike, *On the likelihood of a time series model*, *The Statistician* **27** (1978) 217.
- [50] CHIQCD collaboration, *Muon $g-2$ with overlap valence fermions*, *Phys. Rev. D* **107** (2023) 034513 [[arXiv:2204.01280](#)].
- [51] M. Cè et al., *Window observable for the hadronic vacuum polarization contribution to the muon $g-2$ from lattice QCD*, *Phys. Rev. D* **106** (2022) 114502 [[arXiv:2206.06582](#)].
- [52] EXTENDED TWISTED MASS collaboration, *Lattice calculation of the short and intermediate time-distance hadronic vacuum polarization contributions to the muon magnetic moment using twisted-mass fermions*, *Phys. Rev. D* **107** (2023) 074506 [[arXiv:2206.15084](#)].
- [53] MILC, FERMILAB LATTICE, HPQCD collaboration, *Hadronic vacuum polarization for the muon $g - 2$ from lattice QCD: Complete short and intermediate windows*, *Phys. Rev. D* **111** (2025) 094508 [[arXiv:2411.09656](#)].
- [54] G. Benton, D. Boito, M. Golterman, A. Keshavarzi, K. Maltman and S. Peris, *Data-Driven Determination of the Light-Quark Connected Component of the Intermediate-Window Contribution to the Muon $g-2$* , *Phys. Rev. Lett.* **131** (2023) 251803 [[arXiv:2306.16808](#)].
- [55] S. Kuberski, M. Cè, G. von Hippel, H.B. Meyer, K. Ottnad, A. Risch et al., *Hadronic vacuum polarization in the muon $g - 2$: the short-distance contribution from lattice QCD*, *JHEP* **03** (2024) 172 [[arXiv:2401.11895](#)].
- [56] S. Spiegel and C. Lehner, *High-precision continuum limit study of the HVP short-distance window*, *Phys. Rev. D* **111** (2025) 114517 [[arXiv:2410.17053](#)].

- [57] BELLE collaboration, *Observation of an Excited Ω^- Baryon*, *Phys. Rev. Lett.* **121** (2018) 052003 [[arXiv:1805.09384](#)].
- [58] S. Gusken, U. Low, K.H. Mutter, R. Sommer, A. Patel and K. Schilling, *Nonsinglet Axial Vector Couplings of the Baryon Octet in Lattice QCD*, *Phys. Lett.* **B227** (1989) 266.
- [59] C. Aubin and K. Orginos, *A new approach for Delta form factors*, *AIP Conf. Proc.* **1374** (2011) 621 [[arXiv:1010.0202](#)].
- [60] S. Capstick and N. Isgur, *Baryons in a relativized quark model with chromodynamics*, *Phys. Rev. D* **34** (1986) 2809.
- [61] EXTENDED TWISTED MASS collaboration, *Ratio of kaon and pion leptonic decay constants with $N_f = 2 + 1 + 1$ Wilson-clover twisted-mass fermions*, *Phys. Rev. D* **104** (2021) 074520 [[arXiv:2104.06747](#)].
- [62] N. Miller et al., *Scale setting the Möbius domain wall fermion on gradient-flowed HISQ action using the omega baryon mass and the gradient-flow scales t_0 and w_0* , *Phys. Rev. D* **103** (2021) 054511 [[arXiv:2011.12166](#)].
- [63] MILC collaboration, *Gradient flow and scale setting on MILC HISQ ensembles*, *Phys. Rev. D* **93** (2016) 094510 [[arXiv:1503.02769](#)].
- [64] R. Dowdall, C. Davies, G. Lepage and C. McNeile, *Vus from pi and K decay constants in full lattice QCD with physical u, d, s and c quarks*, *Phys. Rev. D* **88** (2013) 074504 [[arXiv:1303.1670](#)].
- [65] EXTENDED TWISTED MASS collaboration, *Quark masses and decay constants in $N_f = 2 + 1 + 1$ isoQCD with Wilson clover twisted mass fermions*, *PoS LATTICE2019* (2020) 181 [[arXiv:2001.09116](#)].
- [66] FLAVOUR LATTICE AVERAGING GROUP (FLAG) collaboration, *FLAG review 2024*, *Phys. Rev. D* **113** (2026) 014508 [[arXiv:2411.04268](#)].
- [67] M. Di Carlo, D. Giusti, V. Lubicz, G. Martinelli, C.T. Sachrajda, F. Sanfilippo et al., *Light-meson leptonic decay rates in lattice QCD+QED*, *Phys. Rev.* **D100** (2019) 034514 [[arXiv:1904.08731](#)].
- [68] J.D. Hunter, *Matplotlib: A 2d graphics environment*, *Computing in Science & Engineering* **9** (2007) 90.